European Journal of Wood and Wood Products (2025) 83:54
https://doi.org/10.1007/s00107-025-02208-0

ORIGINAL ARTICLE

U-NET-based deep learning for automated detection of lathe checks in homogeneous wood veneers

Caroline Marc[1] · Bertrand Marcon[1] · Louis Denaud[1] · Stéphane Girardon[1]

Received: 14 August 2024 / Accepted: 17 January 2025

Abstract

Automated detection of lathe checks in wood veneers presents significant challenges due to their variability and the natural properties of wood. This study explores the use of two convolutional neural networks (U-Net architecture) to enhance the precision and efficiency of lathe checks detection in poplar veneers. The approach involves sequential application of two U-Nets: the first for detecting lathe checks through semantic segmentation, and the second for refining these predictions by connecting fragmented lathe checks. Post-processing techniques are applied to denoise the mappings and extract precise lathe check characteristics. The first U-Net demonstrated strong performance in predicting lathe check presence, with precision and recall scores of 0.822 and 0.835, respectively. The second U-Net refined predictions by linking disjointed segments, improving the overall lathe checks mapping process. Comparative analysis with manual methods revealed comparable or superior performance of the automated approach, especially for shallow lathe checks. The results highlight the potential of the proposed method for efficient and reliable lathe check detection in wood veneers.

1 Introduction

During the peeling process for veneer production, cracking occurs at the cutting zone due to a combination of various mechanical stresses and especially a traction stress field in front of the knife (Thibaut and Beauchêne 2004). For so-called homogeneous species, this phenomenon tends to be periodic (Denaud et al. 2007; Leney 1959; Thibaut 1988). The depth and frequency of these lathe checks depend on numerous factors, including veneer thickness, wood species, and production parameters (Rohumaa et al. 2018). Lathe checks significantly affect the mechanical properties and gluing capabilities of veneers (DeVallance et al. 2007; Pot et al. 2015; Rahayu et al. 2013; Rohumaa et al. 2013, 2016). Therefore, measuring them is crucial to improve both the veneer grading or gluing into wood engineering products processes.

Historically, lathe checks were measured by impregnating veneers with dye and observing them under a microscope (Lutz 1960; Movassaghi 1985). Due to the cumbersome and time-consuming nature of these measurements, new methods have been developed, particularly acoustic measurements (Tomppo et al. 2009; Wang et al. 2001). Denaud et al. (2007) employed this approach by recording the sound emitted near the knife during the peeling process and the cutting forces, which allowed for the prediction of lathe checks occurrence frequencies. These measurements were then compared with the surface profiles of the veneers, which were obtained by bending them to open the lathe checks and using a distance sensor. Although these measurements provided accurate estimates of lathe checks positions, they did not offer quantitative data on their depth or other geometrical characteristics. Antikainen et al. (2015) developed a method to simultaneously measure wood fiber orientation and lathe checks depths through transillumination imaging of the veneer. The coefficient of determination R^2 of 0.86 with reference values confirms the consistency of this method for measuring depths.

The SMOF ("Système de Mesure d'Ouverture des Fissures", i.e. lathe checks opening measurement system), developed at LaBoMaP (Palubicki et al. 2010), allows for extensive observation and complete mapping of lathe checks geometry in the radial-tangential (RT) plane of the wood. As shown in Fig. 1, imaging is performed on the edge of veneer strips passing over a suitably sized pulley to open the

✉ Caroline Marc
Caroline.Marc@ensam.eu

[1] Arts et Metiers Institute of Technology, LABOMAP, Cluny F-71250, France

Published online: 10 February 2025

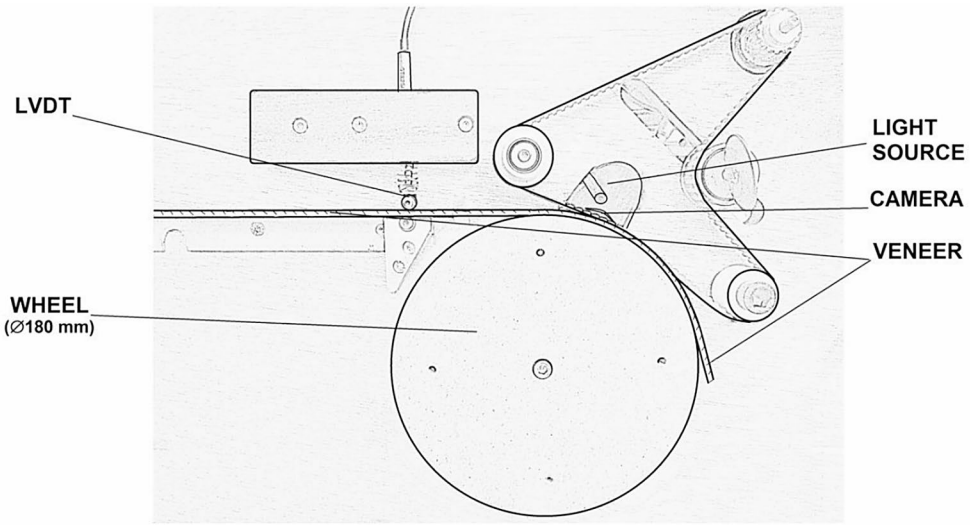

Fig. 1 Lathe checks opening measurement system (SMOF) (Rohumaa et al. 2018) (LVDT = linear variable differential transformer)

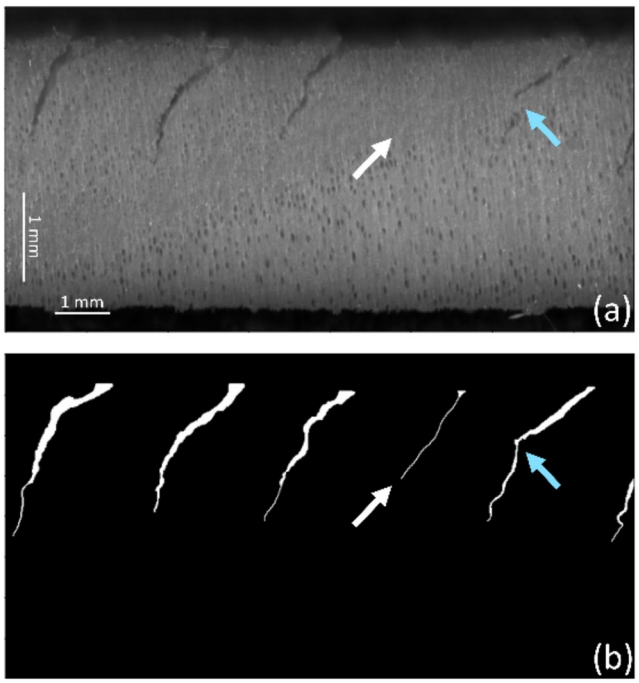

Fig. 2 (**a**) Lathe checks in a poplar veneer arising from the SMOF imaging system, and (**b**) its corresponding lathe checks mask. The white arrow indicates a lathe check that is difficult to discern, and the blue arrow indicates a lathe check that appears discontinuous

lathe checks and make them more visible. The SMOF easily provides images of lathe checks along the entire edge of a veneer, but the automated lathe checks detection via image processing described by Palubicki et al. (2010) does not work well with all types of wood and various lathe checks sizes. Therefore, a manual detection is usually performed; however, Antikainen et al. (2015) demonstrate a significant operator effect on the measurement of lathe checks depth in this kind of images.

The aim of this study is to automate the detection process of lathe checks from images of veneers captured by the SMOF, aiming to save time and enhance the measurement accuracy.

Figure 2 presents an example of a cracked poplar veneer image obtained with the SMOF, along with the corresponding lathe checks mask. While most lathe checks are easily visible to the naked eye, the gray levels of the pixels belonging to lathe checks are similar to those of certain wood details, such as vessels. Furthermore, some lathe checks appear discontinuous (blue arrows) even though they are not, and others are very difficult to discern (white arrows), primarily due to the challenge of obtaining an optimally clean surface for imaging.

There are studies in the literature addressing the detection of lathe checks on the main surface (tangential plane) of veneers (Antikainen et al. 2015) and veneered panels (Burnard et al. 2018). As for studies focusing on cross-sectional images of veneers (transverse plane), these include the work of Palubicki et al. (2010) cited above, and that of Grubîi and Johansson (2021), who detect slicing checks on flat-sliced veneers by image processing of the cross-section after firstly highlighting them with surface staining. Additionally, studies exist on other types of cracks in wood and various materials, which, like wood with its porous structure, have features that complicate image analysis. Crack detection methods can generally be categorized into two groups (Munawar et al. 2021): those based on image processing, and those based on machine learning. In most cases, both categories employ a common approach: cracks detection, for example by semantic segmentation of images, meaning assigning a class to each pixel (1 for a pixel belonging to a crack, 0 for everything else), followed by the extraction of crack parameters.

The basic method for image processing segmentation is grayscale histogram-based thresholding, as demonstrated by Bhandarkar et al. (2002, 1999) for detecting cracks in cross-sectional computed tomography images of logs. However, cracks exhibit geometries and gray levels similar to those of growth rings. Bhandarkar et al. (2005) have used the orientation of the rings to detect cracks, given that cracks are typically perpendicular to the wood rings in cross-sections. They employ Sobel-like operators (Jähne 2005) to detect the rings, followed by fork detection and clustering methods to locate the cracks, achieving better performance than the previous method. Wang and Huang (2010) compare four detection methods in their study: an integrated algorithm (pre-processing before threshold-based segmentation), a morphological approach (mathematical morphology and curvature evaluation), a percolation-based method (model based on the natural phenomenon of liquid permeation), also used in Yamaguchi and Hashimoto (2009), and a practical technique (semi-manual, requiring operator intervention). Their study indicates that the latter method yields the best results, despite requiring human intervention, whereas the effectiveness of the other methods depends heavily on processing parameters and image characteristics.

Machine learning techniques have revolutionized semantic segmentation, thereby enhancing crack detection by providing powerful tools for analyzing complex and varied images. Unlike traditional image processing methods that rely on predefined rules, machine learning approaches learn from annotated data and can adapt to a wide array of scenarios. In supervised learning, algorithms for semantic segmentation are trained on datasets where each pixel is labeled as either a crack or non-crack. Once trained, the model can predict crack presence in new images. Convolutional neural networks (CNNs) (LeCun et al. 2015) are especially effective for such applications (Doğan and Ergen 2022; Ehtisham et al. 2024; He et al. 2020; Lin et al. 2023; Zhang et al. 2016).

In summary, these approaches capitalize on the ability of algorithms to learn complex features and adapt to various detection environments, which is essential for heterogeneous materials like wood. In this study, segmentation will be carried out using a combination of convolutional neural networks, specifically those following the U-Net architecture, which will be described in detail later. This type of network, initially developed for medical imaging (Ronneberger et al. 2015), was selected for its effectiveness in semantic segmentation tasks. The study will then describe the creation of the dataset from images of poplar veneers, a wood considered relatively homogeneous, outline the different stages of the crack detection process, and finally, present the detection performance.

2 Materials and methods

2.1 Data collection

The images studied will be, as previously mentioned, images of poplar veneers (*Populus* × *canadensis*, clone I-214). This species was selected because it is considered homogeneous (at least at a mesoscopic scale relevant to the dimensions of lathe checks and the observation scale), which simplifies automated lathe check detection for these initial tests. Additionally, a large amount of data was already available for this species, including SMOF images produced for previous studies.

To obtain these images, 3 mm thick veneers were peeled from several poplar logs. Various cracking rates were achieved by adjusting the pressure rate of the pressure bar. This bar exerts a compression stress field upstream of the tool in opposition to the traction stress field inherent to the cutting geometry. Therefore, the higher the pressure rate, the more it limits lathe check extension but increases their frequency, before almost eliminating them (Rohumaa et al. 2018). The studied pressure bar rates (PR) range from 5% (deeper, less frequent lathe checks) to 15% (closer, shallower, or even nonexistent lathe checks). This percentage corresponds to the relative distance from the nominal thickness (3 mm) (Lutz 1974), for instance, a 5% rate corresponds to a relative distance of 5% × 3 mm = 0.15 mm below the nominal thickness between the cutting face and the pressure bar nose. Using images with different cracking rates for network training makes them more versatile and efficient.

The SMOF allows imaging of the edge of veneer strips 15 to 40 mm long (longitudinal direction of the wood). For scanning, the veneers were laser-cut into strips to ensure a satisfactory surface condition. The resulting images are 12 bits grayscale images, and their resolution is 112 px.mm^{-1} in the radial direction of the wood (R) and 69 px.mm^{-1} in the tangential direction of the wood (T), which is the strip's direction of movement.

2.2 Detection steps

Figure 3 illustrates the various steps in the proposed lathe check detection method. The input image first passes through two consecutive convolutional neural networks (CNNs), followed by a post-processing stage. The first CNN (U-Net 1) generates a probability map that indicates whether each pixel belongs to a lathe check or not. In some cases, as shown in Fig. 3, the lathe checks appear segmented and thus show up as several groups of non-zero pixels in the U-Net 1 prediction. The next stage, U-Net 2, aims to connect the groups of pixels belonging to the same lathe check.

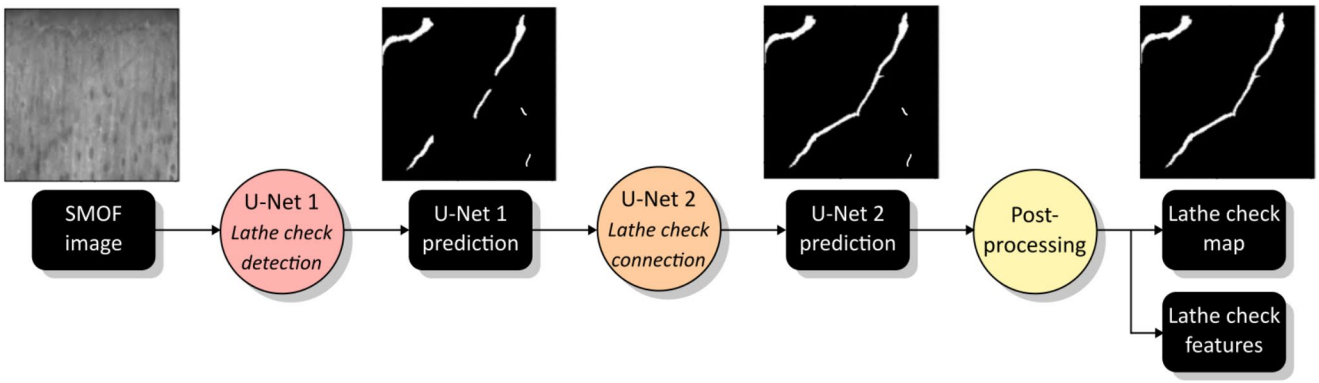

Fig. 3 Block diagram of the lathe checks detection process

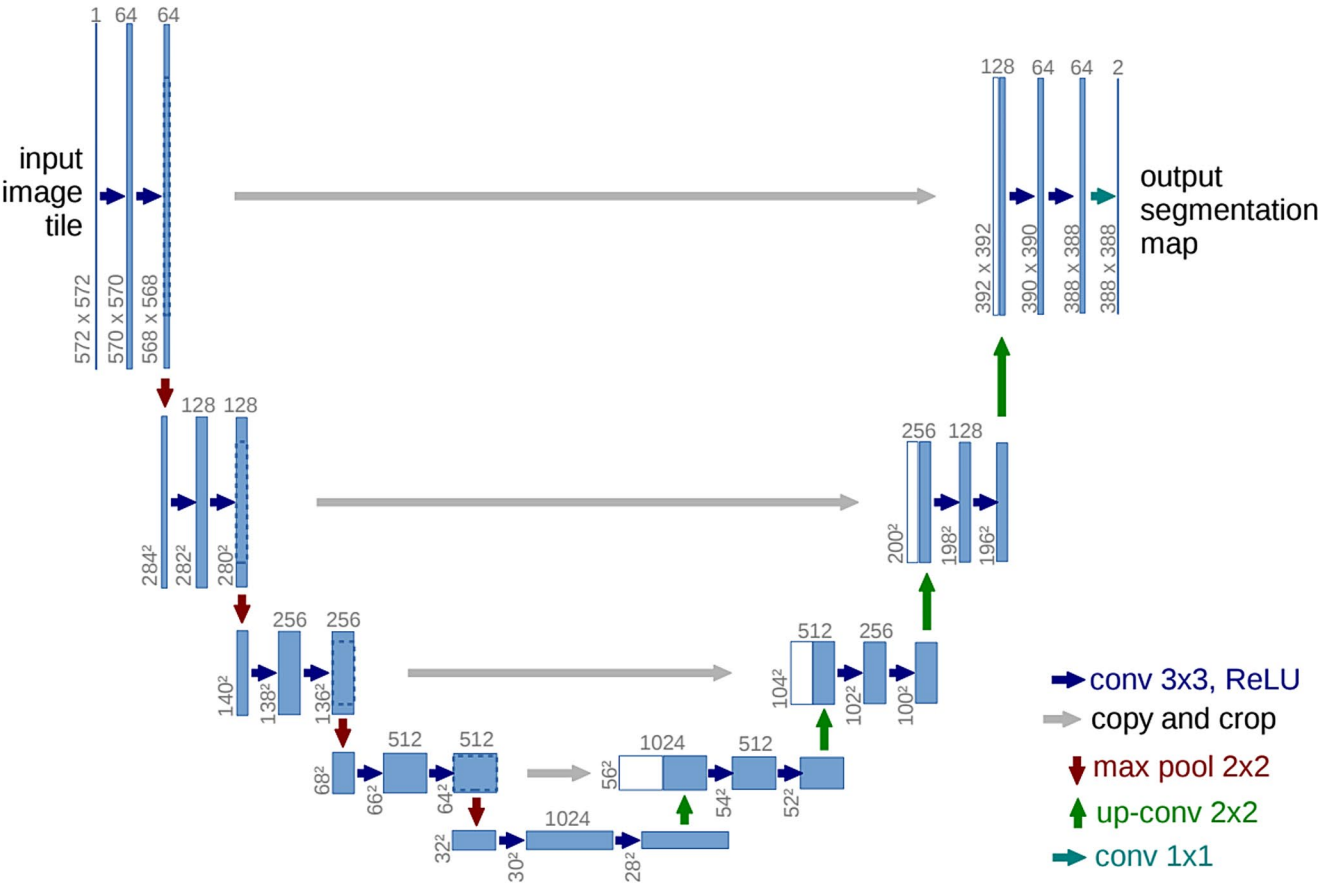

Fig. 4 Example of a U-net architecture, each blue box corresponds to a multi-channel feature card, each white box to a copied card, and the arrows indicate the various operations (Ronneberger et al. 2015)

The final stage, which will be detailed later, produces the final lathe check map and extracts all the characteristics in a tabular form.

2.3 U-Net architecture

The two CNNs utilized in our method are U-Nets, specifically designed for semantic segmentation tasks (Ronneberger et al. 2015). These networks deliver precise and robust results, even with a limited amount of training data. As shown in Fig. 4, a U-Net consists of an encoder part (left side), which reduces the spatial resolution of the image by extracting features, and a decoder part (right side) that restores the resolution while producing a segmentation map. The encoder's features are fused with the decoder's activations to preserve spatial details at different scales, giving the network its characteristic U-shape. The network architecture and its various operations are described in more detail

by Ronneberger et al. (2015). For this study, the network handles input grayscale images of size 256 × 256 pixels (12 bit depth), includes 5 resolution reduction steps followed by 5 resolution enlargement steps, and produces an output image with the same dimensions as the input image.

2.4 Datasets creation

2.4.1 U-Net 1 dataset

Before being able to use a supervised CNN, it is necessary to train it on a dataset composed of grayscale edge images of veneers obtained with the SMOF (input images) and the corresponding binary masks (ground truth), with only black pixels (0) except for those located at a lathe check (white pixels = 1). Five veneer strips were selected for this study: two strips were peeled at a pressure rate of 15% and three at a pressure rate of 10%, allowing the network to be trained to recognize lathe check of different sizes. Each strip is 650 mm wide (tangential direction of the wood). Pixels belonging to a lathe check were manually labeled to create the ground truth masks. A total of 1,135 lathe checks were identified in all these data, with an average area of 497 px² per lathe check, details per strip are given in Table 1.

To finalize the dataset and obtain images with dimensions suitable for the network, a 256 × 256 px² window scans each of the 5 veneer images with a step of 64 pixels in both directions. The 5 veneer images are used with the lathe checks oriented in the same direction (opening to the right, propagation to the left), to enhance the network's performance for a consistent lathe check orientation. This being possible since all lathe checks in a veneer, regardless of their local shape, follow the same orientation. To avoid having a dataset with a too low ratio of white pixels to black pixels (Buda et al. 2018), only the pairs of sub-images where the ground truth contains at least 1 white pixel are kept, as well as 1% of the pairs of sub-images with no lathe checks. A total of 8,040 pairs of sub-images is obtained, with a total ratio of white pixels to black pixels of 1.2%.

Table 1 Dataset strips information. The values in parentheses represent the standard deviation of the values

Strip id	Pressure rate	Number of lathe checks	Average lathe check area [px²]	Number of sub-images
1	15%	166	145 (107)	985
2	15%	159	197 (152)	1,075
3	10%	253	726 (426)	1,990
4	10%	279	720 (484)	2,010
5	10%	278	697 (347)	1,980
	Total	1,135	Total	8,040

2.4.2 U-Net 2 dataset

The process of creating the dataset for the second network mirrors the approach used for the first one. The difference here is that the input images are the predictions made by U-Net 1, which are binary lathe checks prediction maps thresholded at a low value of 0.15 (empirically determined threshold). Three new veneer strips were used for this dataset: two were peeled at a pressure rate of 15% and one at 10%. To create the ground truth masks, white pixels were manually added to connect groups of white pixels belonging to the same lathe checks, as illustrated in Fig. 3. 2,897 white pixels were added to connect 173 lathe checks, which corresponds to 0.6% of the total number of white pixels. The sub-image extraction follows the same procedure as for the first dataset, except that here only the pairs of sub-images containing at least 1 white pixel are retained, yielding a total of 5,272 pairs of sub-images.

2.5 Training parameters and metrics for performance evaluation

For both networks, the dataset images are split into three distinct sets: training data (64%), validation data (16%), and test data (20%). The training data is used to fine-tune the model's weights, the validation data allows for performance monitoring and helps to prevent overfitting during training, and the test data is used to assess the final performance of the model on previously unseen data. The pixel values of the images are normalized between 0 and 1 before training, by dividing them by 256 since the frames have an 8 bit depth.

The training configuration for both U-Nets involves using the Adam optimizer with a learning rate of 0.001, while performance is evaluated using accuracy. The binary cross-entropy loss function is chosen due to its efficacy in binary classification tasks, particularly in dealing with unbalanced datasets where positive instances (lathe checks) are relatively sparse (Li et al. 2021). The model is trained with a batch size of 32 over 20 epochs using TensorFlow, with each epoch taking about one hour to complete, on a system with an Intel Xeon Silver 4210R CPU, 128 GB RAM, and Windows OS Server 2019.

To measure the performance of the segmentation models, the following metrics are introduced (Doğan and Ergen 2022):

- *Precision*:

$$Precision = \frac{TP}{TP + FP} \tag{1}$$

where TP is the number of true positives and FP is the number of false positives. Precision measures the proportion of correct predictions among all the predictions made by the model.

- *Recall*:

$$Recall = \frac{TP}{TP + FN} \tag{2}$$

where FN is the number of false negatives. Recall measures the model's ability to identify all relevant elements (lathe checks pixels).

- *F-score*:

$$F{-}score = 2 \times \frac{Precision \times Recall}{Precision + Recall} \tag{3}$$

The *F-score* is the harmonic mean of precision and recall, offering a balance between these two metrics.

- Intersection over Union (*IoU*):

$$IoU = \frac{|A \cap B|}{|A \cup B|} \tag{4}$$

where A is the set of pixels predicted as positive, and B is the set of actual positive pixels. *IoU* measures the overlap between the predictions and the actual lathe checks.

- Root Mean Square Error (*RMSE*):

$$RMSE = \sqrt{\frac{1}{N}\sum_{i=1}^{N}(\widehat{y_i} - y_i)^2} \tag{5}$$

where $\widehat{y_i}$ is the predicted value and y_i is the actual value. *RMSE* quantifies the average error of the predictions.

2.6 Post-processing

Once a complete image of the cracked veneer is predicted by the two U-Nets, its raw prediction is not yet fully usable, as the groups of white pixels do not all correspond to lathe checks. It is necessary to denoise the map and unify the remaining fragmented lathe checks.

Figure 5 illustrates the different stages of this post-processing. Starting from the original image, the borders of the veneer are determined, and all false-positive pixels located outside these borders are set to zero. Next, a morphological closing operation is performed with a kernel of 20 × 20 px² to connect neighboring groups of white pixels. The next step is to eliminate the remaining false positives. For this,

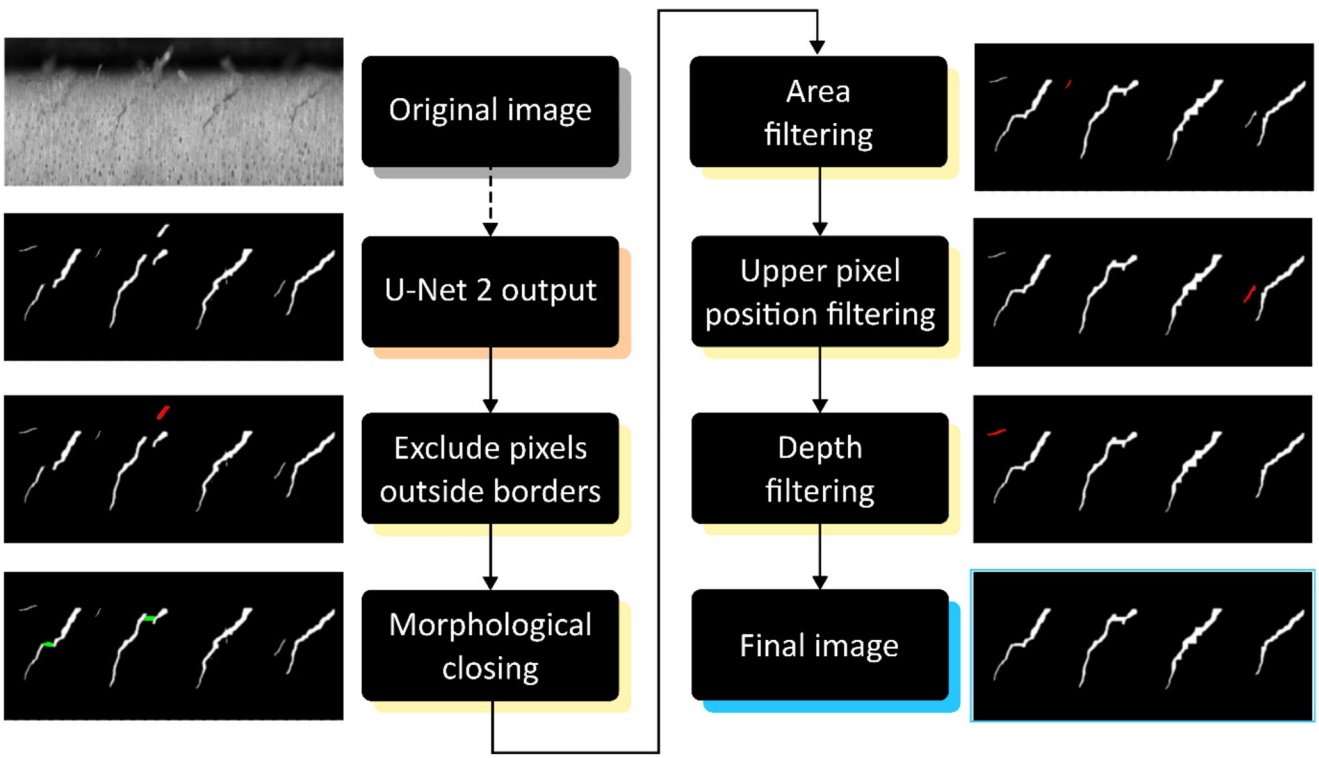

Fig. 5 Post-processing steps: in red the pixels removed by the current process step, and in green the pixels added during the morphological closing step

several filters are applied to the image. First, groups of pixels whose area is not comparable to that of a lathe check, i.e. too small to correspond to a lathe check, are removed. Then, for each remaining group of pixels, the vertical distance between its highest pixel and the veneer's upper edge is measured. Since lathe checks always originate from this upper edge, any group of pixels located further than 56 pixels (representing 16% of the veneer's thickness, empirically determined threshold) from this edge is disregarded. Finally, in theory, in the case of homogeneous wood and stable cutting conditions, lathe checks in the same veneer have relatively similar depths (Rohumaa et al. 2018). Groups of pixels whose depth significantly deviates from the others are filtered out, specifically those with a depth less than the difference between the median depth of the lathe checks in the veneer and their standard deviation. All these thresholds were determined empirically.

Once the final map is obtained, each group of white pixels is considered as a lathe check. Characteristics such as the coordinates of the lathe check (i.e., the position of the highest pixel), its depth (i.e., the distance between the lowest pixel and the upper edge of the veneer), and its area are extracted for all groups of white pixels and recorded as tabular in an easily readable text output file (CSV format).

2.7 Reference measurements

To assess the performance of the proposed method at the veneer level, it is crucial to compare the obtained results with values measured through alternative methods. Two manual techniques are employed in this study. Firstly, the software component of SMOF allows for manual lathe checks detection. The operator identifies each lath check at three points (extremities and middle) in a veneer image, generating a file similar to that of the proposed method, including position and depth values. The term SMOF will hereafter be used to indicate manual detection using the SMOF software. However, the software's limited zoom capability hinders the detection of lathe checks, particularly smaller ones. The second technique, even more tedious, involves examining the veneer images using an inner developed program with Python environment, which allows for as much zooming as necessary and thus providing the most exhaustive list of lathe checks possible. This method is considered the reference measurement.

2.8 Evaluation of method performance

To evaluate the performance of the proposed method, two types of studies were conducted: a repeatability study and a quantitative comparison study.

2.8.1 Repeatability study

In the repeatability study, four operators (A: trained; B, C, and D: untrained) independently detected lathe checks using the SMOF software in three different poplar veneers, obtained from three different pressure rates (PR = 5%, 10%, or 15%). The results from each operator were compared with the reference measurements (performed by operator A) and to the results from our proposed CNNs U-Net method. This comparison allowed us to assess the consistency and reliability of manual detection among different operators, as well as to compare it with the automated method.

To evaluate the different methods statistically, a mode II linear regression (Ludbrook 2010) was performed between these methods and the reference method. Mode II linear regression is a statistical approach used to compare two measurement methods, particularly useful when neither variable can be considered independent. Unlike traditional linear regression, which minimizes errors only along the y-axis, mode II regression minimizes errors on both axes, offering a more balanced estimate of the relationship between the variables. Here, this analysis allows for the determination of whether there is a constant bias (a fixed offset) or a proportional bias (a divergence that increases with the reference value) in the lathe check depths detected by each method (automatic or human operators) compared to the reference depths. The mode II linear regression was performed using the "orthogonal distance regression" algorithm implemented in the SciPy library in Python.

2.8.2 Quantitative comparison study

In the quantitative comparison study, lathe checks detected by an operator (A) using the SMOF and the proposed method in 48 veneers were compared. The 48 veneers were divided into three categories of 16 veneers each, according to the pressure rate used during peeling (PR = 5%, 10%, or 15%). This study involved a significantly larger dataset than the previous study, aiming to provide a more representative assessment of the method's reliability across varying peeling pressure rates. The large number of veneers made it impractical to manually map the lathe checks using the reference method. Instead, the maps produced by the proposed method were analyzed, and the detected lathe checks corresponding to actual lathe checks were counted by the operator A, to study the reliability of this method.

3 Results and discussions

3.1 U-Net 1 performance evaluation

The first U-Net model (U-Net 1) was evaluated using several performance metrics to measure its effectiveness in detecting lathe checks in veneers. The results obtained are summarized in Table 2. The *Precision* of 0.822 indicates that U-Net 1 correctly detects more than 82% of the positive pixels among those it predicted. The *Recall* of 0.835 shows that it manages to identify about 83% of the actual lathe check pixels. The *F-score*, the harmonic mean of *Precision* and *Recall*, is 0.828, indicating a good balance between these two metrics. The *IoU* of 0.707 means that the intersection between the predictions and the actual lathe checks represents about 71% of their total union. Finally, an *RMSE* of 0.055 indicates almost no discrepancy between the predictions and the actual values, which is satisfactory for this task. Overall, these results show that U-Net 1 provides solid performance for predicting pixels belonging to lathe checks.

Figure 6 visually illustrates the performance of U-Net 1 in lathe checks detection. For the three images presented from the test set, the ground truth mask is very similar to the network's prediction, indicating that the lathe checks are accurately detected, even for small and difficult to discern lathe checks, as in the third line.

3.2 U-Net 2 performance evaluation

The metrics for the quantitative evaluation of U-Net 2 are summarized in Table 2. The obtained values show excellent results, significantly better than those for U-Net 1. This can be attributed to the fact that there is a very small difference between the input image and the ground truth, with only 0.6% of positive pixels added to unify certain lathe checks. Therefore, these metrics may not be the most appropriate for quantifying the performance of this model, and the results from the two U-Nets are not directly comparable given their distinct roles in the detection process.

From a qualitative perspective, the network seems to perform well in detecting groups of white pixels belonging to the same lathe check, even when they are relatively far apart, as illustrated in Fig. 7.

Table 2 Performance metrics of the two U-Net models

Metric	U-Net 1	U-Net 2
Precision	0.822	0.989
Recall	0.835	0.979
F-score	0.828	0.984
IoU	0.707	0.968
RMSE	0.055	0.016

3.3 Repeatability study

Figures 8 and 9 present the results of the repeatability study. Figure 8 illustrates the number of detected lathe checks and their depth distributions, categorized by method and operator, and pressure rate. The depth is expressed as a percentage of the lathe check depth relative to the veneer thickness.

A key observation is the disparity in the number of lathe checks detected by operators using SMOF and their depths, corroborating the findings of Antikainen et al. (2015) that the operator significantly influences lathe check detection. Some operators even detect non-existent lathe checks, represented by the non-hatched grey areas, which is also observed in detections using U-Nets, particularly at 15% and 5% pressure rates.

Regarding the number of detected lathe checks, the proposed method identifies an equivalent number to the SMOF operators, except for the smallest lathe checks (PR = 15%), where it significantly outperforms. However, for the deepest lathe checks, our method performs less effectively, likely due to the networks not being trained with veneers obtained at 5% pressure rates.

Regarding the mean depths of the detected lathe checks, as illustrated in Figs. 8 and 9, they fall within similar ranges across the three pressure rate categories. In Fig. 9, each point represents a lathe check, and only those lathe checks common with the reference are represented. As a reminder, the measurements labeled 'Ref' and 'A' are performed by the same operator but with two different methods, which is why the points for operator A are aligned along the x = y line in this figure. The automatically detected lathe checks tend to appear deeper than they are in reality, except for the veneer at PR = 5%, where they are slightly less deep than the reference. In contrast, the other operators tend to consistently detect the lathe checks as less deep than they actually are.

Table 3 provides a detailed summary of the linear regression results from the mode II analysis for lathe check depths detected by each operator and by the U-Net method, relative to the reference depth, across three different pressure rates (5%, 10%, and 15%). These results allow for assessing the existence of fixed bias (as indicated by the intercept) and proportional bias (as indicated by the slope) in the detection methods, along with their level of significance. The slope indicates proportional bias: if the slope deviates from 1, it suggests that the method tends to under- or overestimate the depth depending on the reference value. The intercept reveals fixed bias, where non-zero values indicate a consistent under- or overestimation regardless of depth.

The findings suggest that for the U-Nets model, the slope values at 10% and 5% pressure rates are statistically significant (p-value < 0.05). This indicates a proportional bias where the detection depth progressively diverges from the

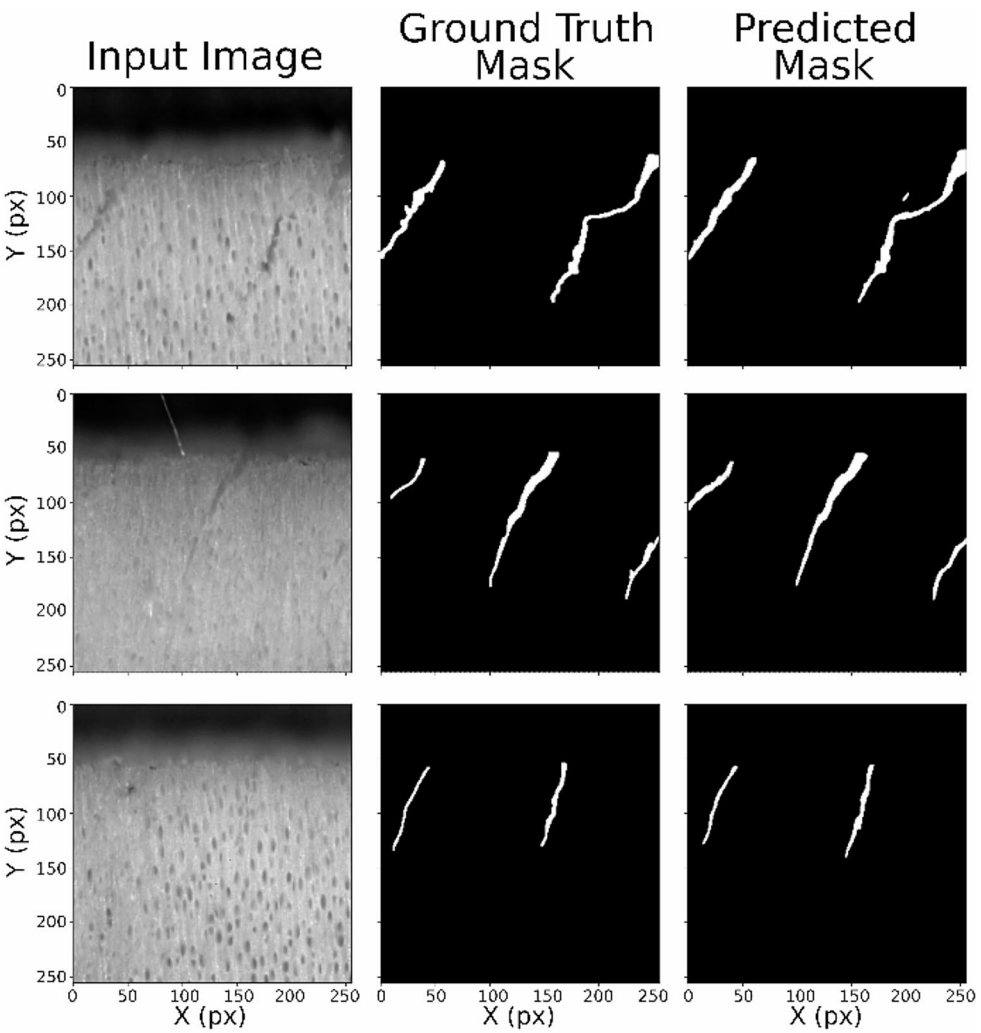

Fig. 6 U-Net 1 predictions of test batch images, from images of veneer peeled with PR at 10%, 10% and 15% from top to bottom

reference, particularly for the 10% pressure rate with a slope of 1.25, suggesting that as lathe check depth increases, the U-Nets model tends to detect lathe checks deeper than the reference. The slope at the 15% pressure rate is not statistically significant (p-value > 0.05), indicating no proportional bias at this pressure rate. The intercept values across all pressure rates (15%, 10%, and 5%) are not statistically significant (p-value > 0.05), indicating the absence of a fixed bias, as the U-Nets model does not consistently detect lathe checks deeper or shallower than the reference.

For operators, the slope values are generally close to 1, especially at the lower pressure rates (10% and 5%), indicating limited proportional bias for most operators under these conditions. However, operators B and D show deviations from this trend, with slopes differing significantly from 1 in certain cases, pointing to proportional bias in their detections. Fixed bias is indicated by the intercepts, with significant values for several operators at different pressure rates. Operators B and C, in particular, tend to consistently under-detect lathe checks across depths.

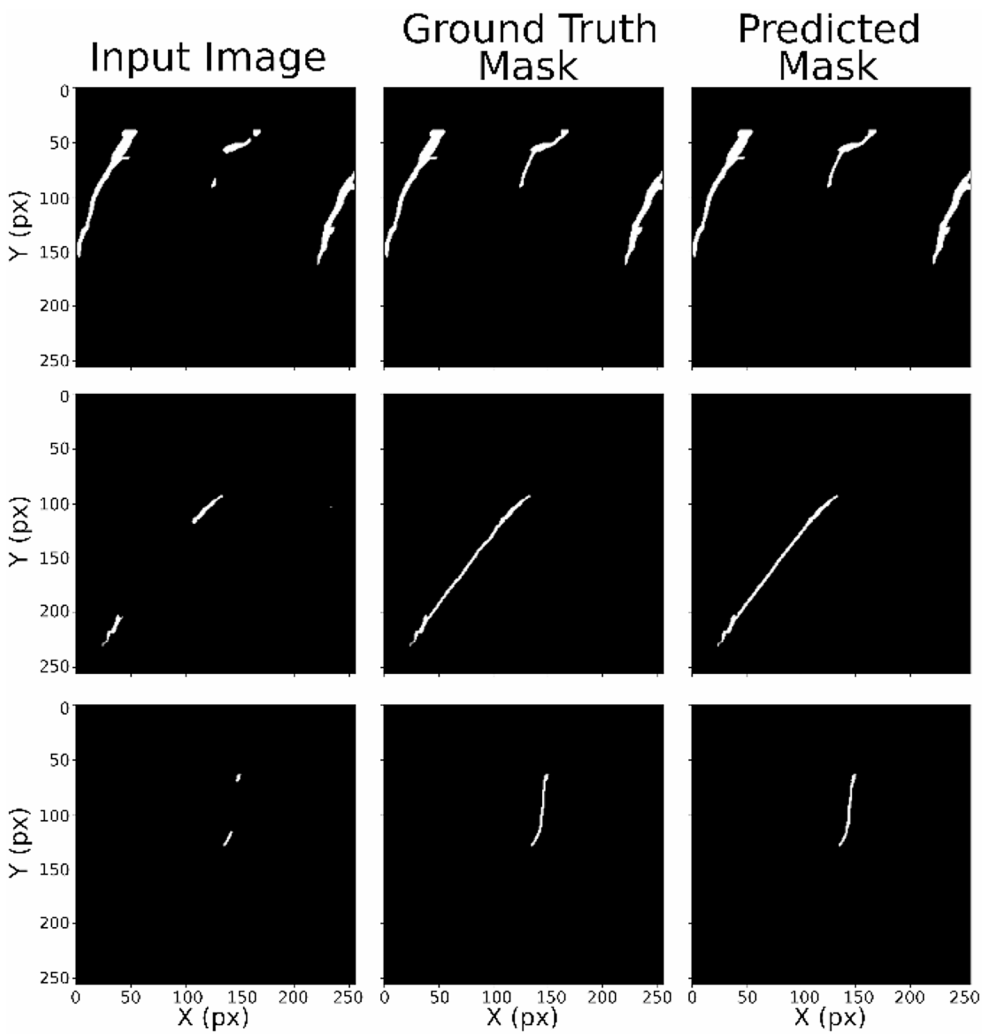

Fig. 7 U-Net 2 predictions of test batch image

3.4 Quantitative comparison study

In this study, only two methods are compared, but for a number of lathe checks at least 10 times higher than in the previous study to ensure more representative results. Figures 10 and 11 illustrate the findings from this comparative study. As observed in the literature (Denaud et al. 2007; Leney 1959; Thibaut 1988), the average depth and the number of checks per given length are inversely proportional. At 5% PR, the number of lathe checks detected automatically is slightly lower than manual detection. However, for the other two PRs, it is significantly higher, exceeding manual detection by more than three times at 15% PR. Additionally, upon verifying the lathe checks maps generated by the proposed method, it was confirmed that the automatically detected lathe checks correspond to actual lathe checks. This is represented by the grey hatching in the figure and accounts for nearly all the lathe checks, with at least 95% being correctly identified. The significantly poorer performance of manual detection with the SMOF for the 15% and 10% PR can be explained by the difficulty of discerning certain lathe checks (see Fig. 2), particularly the smaller ones.

Concerning the depth of the detected lathe checks, it is evident once again that the developed model tends to detect lathe checks as being deeper than those identified manually. For the three pressure rates considered, the average depth discrepancy for the common lathe checks is approximately 10%.

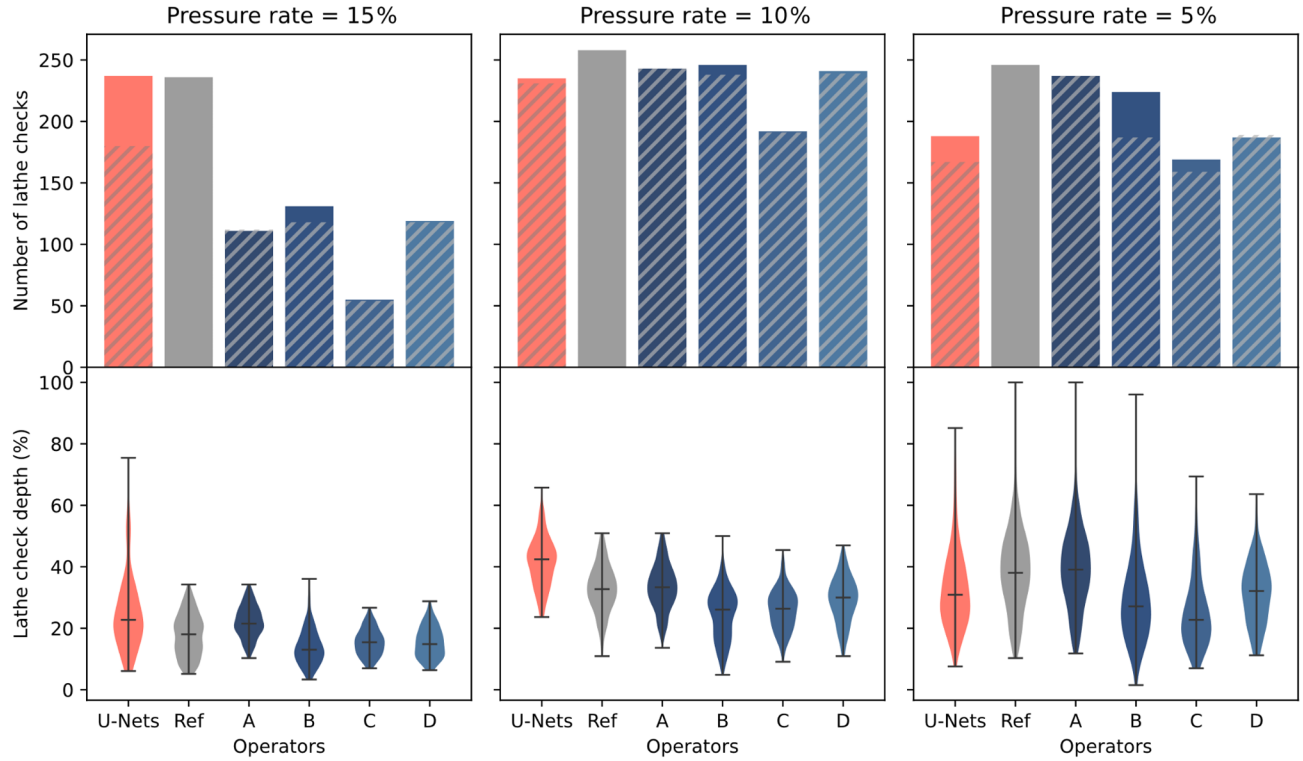

Fig. 8 Comparison of the number of lathe checks detected (top row) and the distribution of lathe check depths (bottom row) across different pressure rates (15%, 10%, and 5%), for lathe checks detected with the proposed method (U-Nets), the reference method and the SMOF by four operators. The grey hatching represents the number of lathe checks in common with the reference

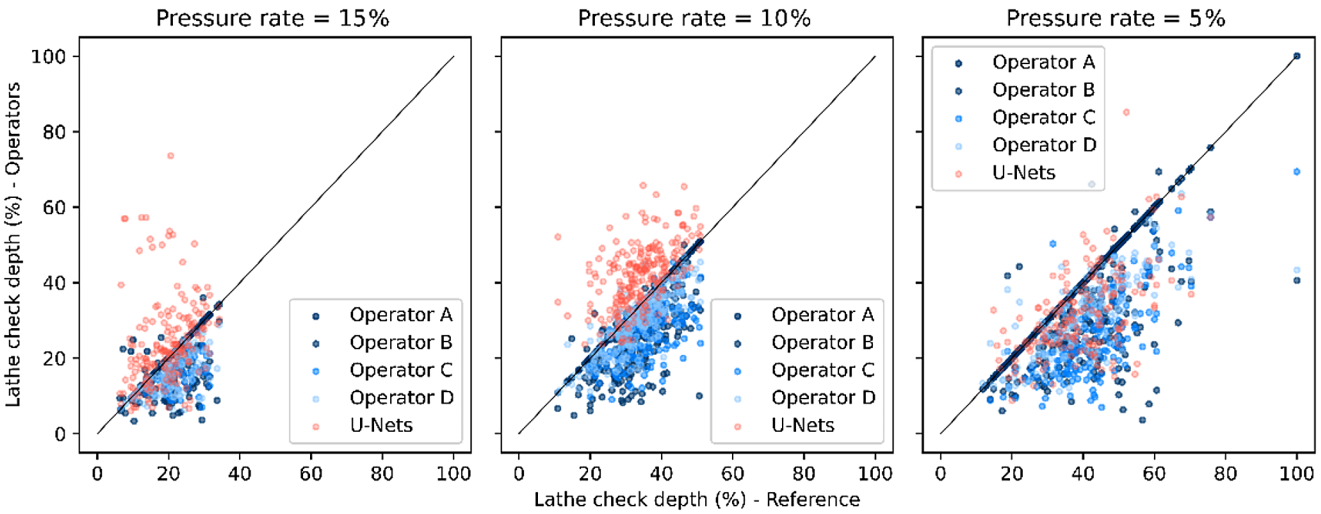

Fig. 9 Scatter plot of lathe checks depths detected by each operator and by the proposed method as a function of the reference depth, for lathe checks in common

4 Discussions

The results obtained with the two U-Net networks demonstrate notable efficiency in detecting lathe checks in wood veneers. U-Net 1, while showing slightly lower metrics compared to U-Net 2, exhibits good detection capability with high precision and recall. U-Net 2, on the other hand, achieves excellent performance, which can be attributed to the low variability of pixels between the input image and the ground truth.

The repeatability study revealed significant disparities in lathe checks detection among different operators using the

Table 3 Mode II linear regression results of lathe checks depths detected by each operator and by the proposed method as a function of the reference depth at various pressure rates (5%, 10%, and 15%): the slope and intercept values, along with their significance levels (p-values). Statistical significance is indicated by asterisks: *** for p-value < 0.001, ** for p-value < 0.01, and * for p-value < 0.05

Pressure rate	Detection method	Slope	Significance (Slope)	Intercept	Significance (Intercept)
15%	U-Nets	5.60		-85.28	
	Operator A	0.95	***	1.22	
	Operator B	0.65	***	0.61	
	Operator C	0.82	***	-4.27	
	Operator D	0.75	***	-0.25	
10%	U-Nets	1.25	***	-0.79	
	Operator A	1.00	***	0.00	***
	Operator B	1.09	***	-11.64	***
	Operator C	0.96	***	-7.56	*
	Operator D	0.95	***	-2.25	
5%	U-Nets	0.96	***	-6.17	
	Operator A	1.00	***	0.00	***
	Operator B	0.97	***	-12.66	*
	Operator C	0.91	***	-13.62	***
	Operator D	0.76	***	0.00	

SMOF software, confirming the operator's impact on detection results. Operators also tend to detect false positives, i.e., non-existent lathe checks, a phenomenon also observed with the proposed method, especially for the pressure rates of 15% and 5%.

Quantitative analysis comparing the results of the proposed method with those obtained manually shows that the U-Nets detect a higher number of true positive lathe checks, particularly for veneers with small-sized lathe checks. However, the automatically detected lathe checks tend to be slightly deeper than those detected manually.

These observations suggest that the convolutional neural network-based approach, while highly effective, could benefit from future adjustments to better align the detected lathe check depths with reality. An interesting perspective would be to train the models with additional and varied data to improve their robustness and reduce false positives. Exploring other CNN architectures, such as R-CNN (Bharati and Pramanik 2020) or ResNet (He et al. 2016), could address some of these limitations and further enhance the model's performance. It may also be advantageous to improve the post-processing part of the method, based on empirically

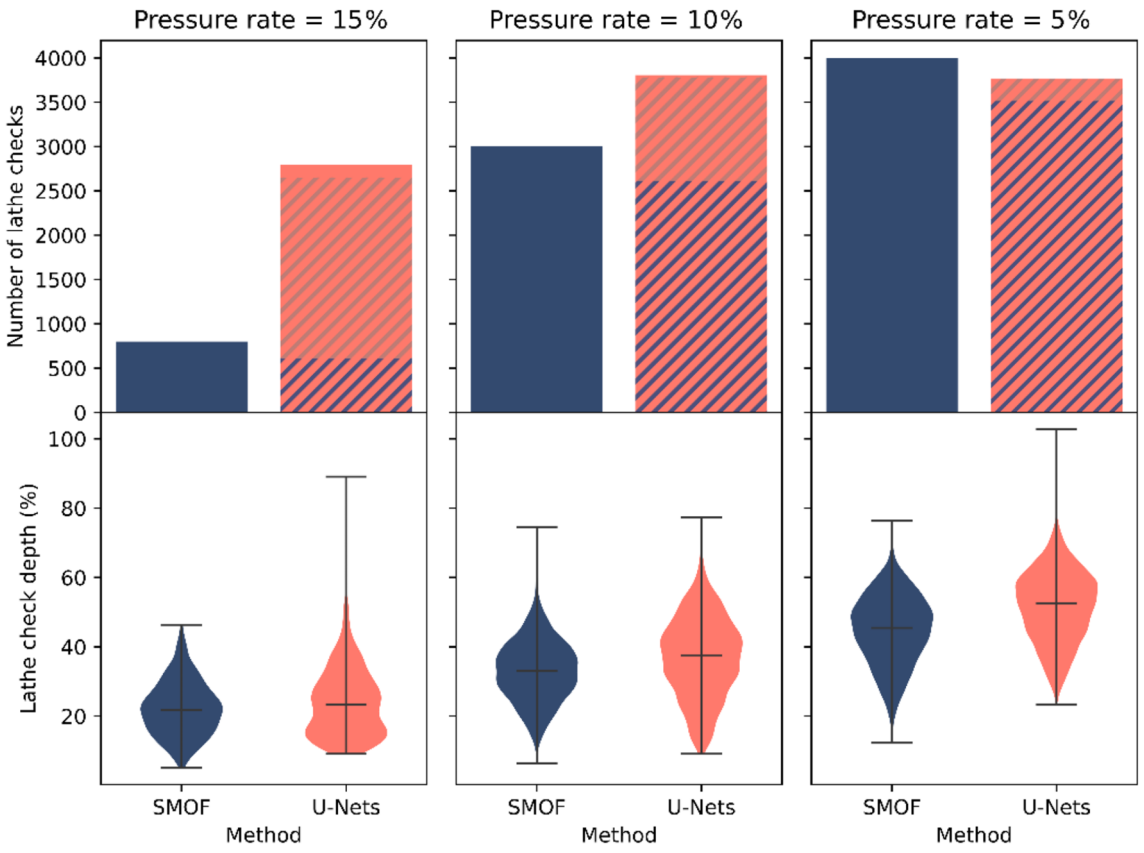

Fig. 10 Comparison of the number of lathe checks detected (top row) and the distribution of lathe check depths (bottom row) across different pressure rates (PR = 15%, 10%, and 5%), for lathe checks detected with the proposed method (U-Nets) and the SMOF. The grey hatching represents the number of lathe checks in common with the reference, and the blue hatching represents the number of lathe checks in common with the SMOF measurement

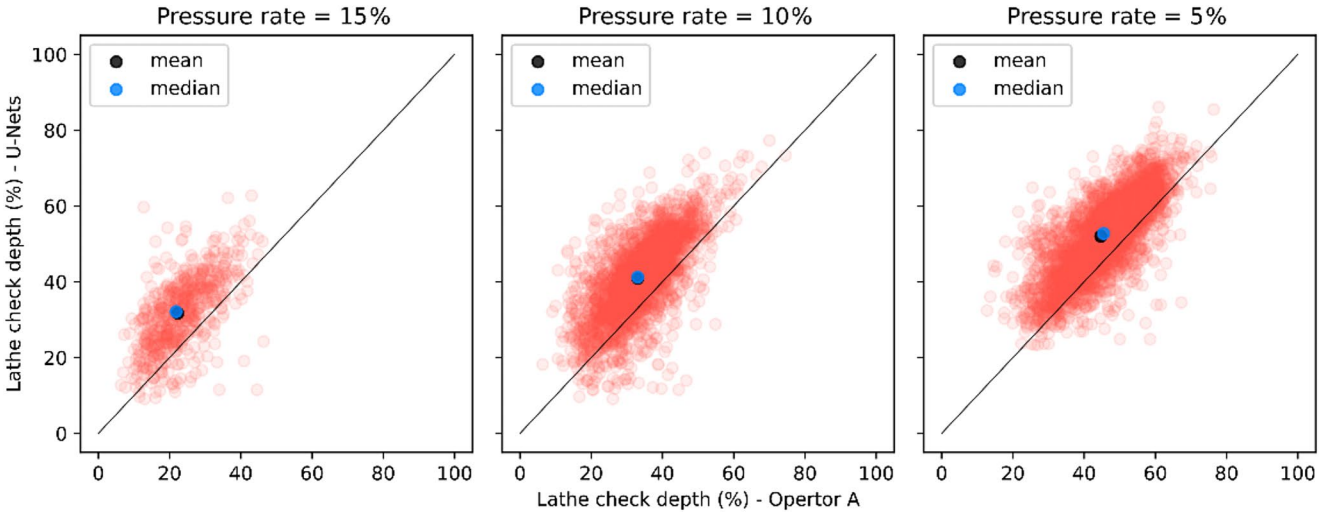

Fig. 11 Scatter plot of lathe checks depths detected by the proposed method as a function of lathe checks depths detected by operator A using the SMOF software, for lathe checks in common

determined parameters (kernel size for the morphological closing and different filter thresholds).

5 Conclusion

Automated detection of lathe checks in wood veneers is a major challenge due to the variability of lathe checks features and the unique visual-pattern characteristics of the wood (presence of fibers, vessels, growth rings…) in comparison to visual homogeneous materials. This study demonstrated the effectiveness of using U-Net based convolutional neural networks to improve the accuracy and efficiency of this task on poplar veneers. The results indicate that the two U-Nets, used sequentially and combined with post-processing, enable robust and precise lathe check detection, surpassing traditional manual methods, especially for small lathe checks.

The first U-Net demonstrated a good ability to predict the presence of lathe checks, with solid performance. The second U-Net refined these predictions by connecting disjointed lathe check segments, thereby demonstrating its usefulness in improving lathe checks mapping.

The proposed method was compared to manual methods, revealing disparities in lathe check detection among operators who are more or less trained on lathe check detection. However, automated detection showed comparable or even superior performance, especially for shallower lathe checks.

In conclusion, automating lathe check detection using deep learning techniques, such as U-Nets, represents a significant advancement for the wood industry perspective on usage. It not only saves time (depending on the performance of the computer used, automated detection takes about as long as manual detection but can be parallelized and does not require active manual work) and improves measurement accuracy, but also reduces variability due to human intervention. Future improvements could include training the networks with images of veneers exhibiting even more varied lathe check rates to further increase their robustness and adaptability. It will also be necessary to test this method on other wood species, particularly those less homogeneous than poplar, to increase the method's versatility and expand its potential applications. It will also allow an assessment of whether it is better to use a model trained on several species, or one specialized by species. Very promising preliminary tests, not presented in this study, were conducted on Douglas fir veneers, a species much less homogeneous in structure at this mesoscopic scale.

Acknowledgements This study is funded by the ANR-21-CE43-0008-02 BOOST project. The authors thank the technical platform Xylomat of the scientific network Xylomat financed by the ANR-10-EQPX-16 XYLOFOREST, which was largely used to carry out this study. They also express their gratitude to the operators who manually detected the lathe check, providing essential data for the validation of the automated detection methods.

Author contributions C. M. developed the methodology, wrote the original draft, and handled data curation. B. M., L. D., and S. G. supervised the project and contributed to the review and editing of the manuscript. All authors reviewed and approved the final version of the manuscript.

Funding Open access funding provided by Arts et Metiers Institute of Technology.

Data availability No datasets were generated or analysed during the current study.

Declarations

Competing interests The authors declare no competing interests.

References

Antikainen T, Eskelinen J, Rohumaa A, Vainio T, Hughes M (2015) Simultaneous measurement of lathe check depth and the grain angle of birch (Betula pendula Roth) veneers using laser transillumination imaging. Wood Sci Technol 49:591–605. https://doi.org/10.1007/s00226-015-0718-8

Bhandarkar SM, Faust TD, Tang M (1999) CATALOG: a system for detection and rendering of internal log defects using computer tomography. Mach Vis Appl 11:171–190. https://doi.org/10.1007/s001380050100

Bhandarkar SM, Faust TD, Tang M (2002) Design and prototype development of a computer vision-based lumber production planning system. Image Vis Comput 20:167–189. https://doi.org/10.1016/S0262-8856(01)00087-7

Bhandarkar SM, Luo X, Daniels R, Tollner EW (2005) Detection of cracks in computer tomography images of logs. Pattern Recognit Lett 26:2282–2294. https://doi.org/10.1016/j.patrec.2005.04.004

Bharati P, Pramanik A (2020) Deep learning Techniques—R-CNN to Mask R-CNN: a Survey. In: Das AK, Nayak J, Naik B, Pati SK, Pelusi D (eds) Computational intelligence in Pattern Recognition. Springer Singapore, Singapore, pp 657–668

Buda M, Maki A, Mazurowski MA (2018) A systematic study of the class imbalance problem in convolutional neural networks. Neural Netw 106:249–259. https://doi.org/10.1016/j.neunet.2018.07.011

Burnard MD, Muszyński L, Leavengood S, Ganio L (2018) An optical method for rapid examination of check development in decorative plywood panels. Eur J Wood Prod 76:1367–1377. https://doi.org/10.1007/s00107-018-1327-7

Denaud LE, Bleron L, Ratle A, Marchal R (2007) Online control of wood peeling process: Acoustical and vibratory measurements of lathe checks frequency. Ann Sci 64:569–575

DeVallance D, Funck J, Reeb J (2007) Douglas-fir plywood gluebond quality as influenced by veneer roughness, lathe checks, and annual ring characteristics. Prod J 57:21

Doğan G, Ergen B (2022) A new mobile convolutional neural network-based approach for pixel-wise road surface crack detection. Measurement 195:111119. https://doi.org/10.1016/j.measurement.2022.111119

Ehtisham R, Qayyum W, Camp CV, Plevris V, Mir J, Khan QZ, Ahmad A (2024) Computing the characteristics of defects in wooden structures using image processing and CNN. Autom Constr 158:105211. https://doi.org/10.1016/j.autcon.2023.105211

Grubîi V, Johansson J (2021) An image processing algorithm for detection and analysis of slicing checks. Eur J Wood Prod. https://doi.org/10.1007/s00107-021-01672-8

He K, Zhang X, Ren S, Sun J (2016) Deep residual learning for image recognition. Presented at the Proceedings of the IEEE conference on computer vision and pattern recognition, pp. 770–778

He T, Liu Y, Yu Y, Zhao Q, Hu Z (2020) Application of deep convolutional neural network on feature extraction and detection of wood defects. Measurement 152:107357. https://doi.org/10.1016/j.measurement.2019.107357

Jähne B (2005) Digital image processing. Springer Science&Business Media. ed

LeCun Y, Bengio Y, Hinton G (2015) Deep Learn Nat 521:436–444. https://doi.org/10.1038/nature14539

Leney L (1959) A photographic study of veneer formation. Forest Prod. J. 10(3):133–139

Li M, Zhang X, Chen J, Thrampoulidis C, Oymak S (2021) AutoBalance: optimized loss functions for Imbalanced Data. 35th Conf Neural Inf Process Syst NeurIPS 34:3163–3177

Lin Y, Xu Z, Chen D, Ai Z, Qiu Y, Yuan Y (2023) IEEECAA J Autom Sin 10:1510–1512. https://doi.org/10.1109/JAS.2023.123357. Wood Crack Detection Based on Data-Driven Semantic Segmentation Network

Ludbrook J (2010) Linear regression analysis for comparing two measurers or methods of measurement: but which regression? Clin. Exp Pharmacol Physiol 37:692–699

Lutz JF (1960) Heating veneer bolts to improve quality of Douglas-fir plywood (Rapport d'étude)

Lutz JF (1974) Techniques for peeling, slicing, and drying veneer. For. Prod Lab For Serv US Dep Agric. 68

Movassaghi E (1985) Influence des paramètres microdensitométriques du bois sur les efforts de coupe et la qualité des placages de Douglas et de Châtaignier obtenus par déroulage (Influence of wood microdensitometric parameters on cutting forces and the quality of Douglas fir and chestnut veneers obtained by peeling). Thesis, Nancy

Munawar HS, Hammad AWA, Haddad A, Soares CAP, Waller ST (2021) Image-Based Crack Detect Methods: Rev Infrastruct 6:115. https://doi.org/10.3390/infrastructures6080115

Palubicki B, Marchal R, Butaud J-C, Denaud LE, Bleron L, Collet R, Kowaluk G (2010) A method of lathe checks measurement; SMOF device and its software. Eur J Wood Prod 10:151

Pot G, Denaud LE, Collet R (2015) Numerical study of the influence of veneer lathe checks on the elastic mechanical properties of laminated veneer lumber (LVL) made of beech. Holzforschung 69:247–316. https://doi.org/10.1515/hf-2014-0011

Rahayu I, Denaud L, Butaud JC, Pot G (2013) Qualités technologiques des panneaux contreplaqués et LVL réalisés avec les nouveaux cultivars de peuplier. (Technological qualities of plywood and LVL panels made with new poplar cultivars)-Entrep 39–42

Rohumaa A, Hunt CG, Hughes M, Frihart CR, Logren J (2013) The influence of lathe check depth and orientation on the bond quality of phenol-formaldehyde–bonded birch plywood. Holzforschung 67:779–786

Rohumaa A, Antikainen T, Hunt CG, Frihart CR, Hughes M (2016) The influence of log soaking temperature on surface quality and integrity performance of birch veneer. Wood Sci Technol 50:463–474. https://doi.org/10.1007/s00226-016-0805-5

Rohumaa A, Viguier J, Girardon S, Krebs M, Denaud L (2018) Lathe check development and properties: effect of log soaking temperature, compression rate, cutting radius and cutting speed during peeling process of European beech (Fagus sylvatica L.) veneer. Eur J Wood Prod 76:1653–1661. https://doi.org/10.1007/s00107-018-1341-9

Ronneberger O, Fischer P, Brox T (2015) U-Net: Convolutional Networks for Biomedical Image Segmentation. Presented at the Medical Image Computing and Computer-Assisted Intervention–MICCAI 2015: 18th International Conference, Springer International Publishing, Munich, Germany, (pp. 234–241)

Thibaut B (1988) Le processus de coupe du bois par déroulage (Thèse). Universite des sciences et techniques du Languedoc, Montpellier, France

Thibaut B, Beauchêne J (2004) Links between Wood Machining Phenomena and Wood Mechanical Properties: The Case of 0°/90° Orthogonal Cutting of Green Wood. Presented at the Proceedings of the 2nd Int. Symposium on Wood Machining, na, Vienna, Austria, pp 149–160

Tomppo L, Tiitta M, Lappalainen R (2009) Ultrasound evaluation of lathe check depth in birch veneer. Eur J Wood Prod 67:27–35

Wang P, Huang H (2010) Comparison Analysis on Present Image-based Crack Detection Methods in Concrete Structures. 3rd Int. Congr. Image Signal Process. CISP2010

Wang J, Biernacki J, Lam F (2001) Nondestructive evaluation of veneer quality using acoustic wave measurements. Wood Sci Technol 34:505–516

Yamaguchi T, Hashimoto S (2009) Fast crack detection method for large-size concrete surface images using percolation-based image processing. Mach Vis Appl 21:797–809. https://doi.org/10.1007/s00138-009-0189-8

Zhang L, Yang F, Zhang YD, Zhu YJ (2016) Road crack detection using deep convolutional neural network, in: IEEE. Presented at the 2016 IEEE international conference on image processing (ICIP), pp. 3708–3712